PHYSICAL REVIEW B **80**, 045413 (2009)

Plasmonic excitations in tight-binding nanostructures

Rodrigo A. Muniz* and Stephan Haas
Department of Physics and Astronomy, University of Southern California, Los Angeles, California 90089-0484, USA

A. F. J. Levi
Department of Electrical Engineering, University of Southern California, Los Angeles, California 90089-0082, USA

Ilya Grigorenko
Theoretical Division T-11, Center for Nonlinear Studies and Center for Integrated Nanotechnologies, Los Alamos National Laboratory, Los Alamos, New Mexico 87545, USA

(Received 20 March 2009; revised manuscript received 28 May 2009; published 15 July 2009)

We explore the collective electromagnetic response in atomic clusters of various sizes and geometries. Our aim is to understand, and hence to control, their dielectric response based on a fully quantum-mechanical description which captures accurately their relevant collective modes. The electronic energy levels and wave functions, calculated within the tight-binding model, are used to determine the nonlocal dielectric response function. It is found that the system shape, the electron filling, and the driving frequency of the external electric field strongly control the resonance properties of the collective excitations in the frequency and spatial domains. Furthermore, it is shown that one can design spatially localized collective excitations by properly tailoring the nanostructure geometry.

DOI: 10.1103/PhysRevB.80.045413 PACS number(s): 73.22.−f, 73.20.Mf, 36.40.Gk, 36.40.Vz

I. INTRODUCTION

Recent advances in nanoscience have created a vast number of experimentally accessible ways to configure atomic and molecular clusters into different geometries with strongly varying physical properties. Specifically, exquisite control of the shape and size of atomic and molecular clusters has made it now possible to investigate the collective electromagnetic response of ultrasmall metal and semiconductor particles.[1,2] The aims of this study are to model and examine plasmonic excitations in such structures and thus to gain an understanding of the quantum-to-classical crossover of collective modes with increasing cluster size. There is obvious technological relevance to tunable collective modes in nanostructures. For example, surface plasmon resonances in metallic nanospheres and films have been found to be highly sensitive to nearby microscopic objects and hence are currently investigated for potential sensing applications.[3] In this context, it is desirable to design customized nanostructures with specifically tailored resonance properties,[4] and this study is intended to be a step into this direction.

It is natural to expect that in many cases the electromagnetic response of nanoclusters is considerably different from the bulk. In particular for very small clusters, the quantum properties of electrons confined in the structure need to be taken into account.[5] Moreover, unlike in the bulk, the coupling between single-particle excitations and collective modes can be very strongly affected by its system parameters. This exponential sensitivity opens up excellent opportunities to optimize the dielectric response via tuning the cluster geometry and its electron filling. For example, by proper arrangement of atoms on a surface one can design nanostructures with controllable resonances in the near infrared or visible frequency range.[2] A possible application of such nanostructures is the creation of metamaterials with negative refractive index at a given frequency. Furthermore, since geometry optimization of bulk resonators has demonstrated minimization of losses in metamaterials,[6] it is also interesting to investigate the effect of the nanostructure shape on the loss function at a given resonance frequency.

To approach this problem, in this study we investigate the formation of resonances in generic systems of finite conducting clusters and examine how their frequency and spatial dielectric response depends on the system size and geometry. In particular, the nonlocality of the dielectric response function in these structures is important and will therefore be properly accounted for. A similar analysis for the case of small *metallic* nanostructures was performed recently using an effective mass approximation.[7] Here we focus on the opposite limit, namely, we assume that electrons in the cluster can be effectively described using a tight-binding model.[8] Because of the more localized nature of the electronic wave functions in this model the overall magnitude of the collective modes is expected to be strongly suppressed as compared to metallic clusters.

This paper is organized in the following way. In Sec. II we introduce the model and method. For a more extended discussion, the reader is referred to Ref. 7, where the same calculations were done for other models such as effective mass and particle in a box. Results for the induced energy as a function of the driving frequency of an externally applied electric field and the corresponding spatial modulations of the charge density distribution function are discussed in Sec. III. Finally, a discussion of possible extensions and applications is given in Sec. IV.

II. MODEL

The interaction of electromagnetic radiation with nanoscale conducting clusters is conventionally described by

semiclassical Mie theory.[9] This is a local continuum-field model which uses empirical values of the linear optical response of the corresponding bulk material and has been applied in nanoparticles to describe plasmon resonances.[10] However, such a semiempirical continuum description breaks down beyond a certain degree of roughness introduced by atomic length scales and thus cannot be used to describe ultrasmall systems. In addition, near-field applications, such as surface-enhanced Raman scattering,[11] are most naturally described using a real-space theory which includes the nonlocal electronic response of inhomogeneous structures. Therefore, we will use a recently developed self-consistent and fully quantum-mechanical model which fully accounts for the nonlocality of the dielectric response function.[7]

Specifically, to identify the plasmonic modes in small clusters we calculate the total induced energy due to an applied external electric field with driving frequency ω and scan for the resonance peaks. The induced energy is determined within the nonlocal linear response approximation.

To keep the computational complexity of this procedure at a minimum, we use a one-band tight-binding model to obtain the electronic energy levels E_i and wave functions $\psi_i(\mathbf{r})$ as a linear combination of s orbitals,

$$\psi_i(\mathbf{r}) = \sum_{i,j} \alpha_{ij} \varphi(\mathbf{r} - \mathbf{R_j}), \tag{1}$$

where $\varphi(\mathbf{r}-\mathbf{R_j})$ is the wave function of an s orbital around an atom localized at position $\mathbf{R_j}$ and α_{ij} are the coefficients of the eigenvector (with energy E_i) of the Hamiltonian, which has the matrix elements

$$\langle \varphi(\mathbf{r} - \mathbf{R_i}) | H | \varphi(\mathbf{r} - \mathbf{R_j}) \rangle = \begin{cases} \mu & \text{for } i = j \\ -t & \text{for } i, jnn. \\ 0 & \text{otherwise.} \end{cases} \tag{2}$$

Here t is the tight-binding hopping parameter which determines the width of the electronic band by $4t$ and μ is the on-site potential that corresponds to the electronic energy at the center of the band. Throughout this paper we set $\mu=0$ and $t=1$, such that the energy levels are measured relative to the center of the band, and the energy scale is given by the hopping parameter. The Hamiltonian matrix is diagonalized using the Householder method to first obtain a tridiagonal matrix and then a QL algorithm for the final eigenvectors and eigenvalues.[12]

Once the electronic wave functions have been obtained, it is possible to calculate the dielectric susceptibility $\chi(\mathbf{r}, \mathbf{r}', \omega)$ via

$$\chi(\mathbf{r}, \mathbf{r}', \omega) = \sum_{i,j} \frac{f(E_i) - f(E_j)}{E_i - E_j - \omega - i\gamma} \psi_i^*(\mathbf{r}) \psi_i(\mathbf{r}') \psi_j^*(\mathbf{r}') \psi_j(\mathbf{r}). \tag{3}$$

The induced charge density distribution function is then obtained by

$$\rho_{ind}(\mathbf{r}, \omega) = \int \chi(\mathbf{r}, \mathbf{r}', \omega) [\phi_{ind}(\mathbf{r}', \omega) + \phi_{ext}(\mathbf{r}', \omega)] d\mathbf{r}', \tag{4}$$

where in turn the induced potential is given by

$$\phi_{ind}(\mathbf{r}, \omega) = \int \frac{\rho_{ind}(\mathbf{r}', \omega)}{|\mathbf{r} - \mathbf{r}'|} d\mathbf{r}'. \tag{5}$$

We avoid the large memory requirement to store $\chi(\mathbf{r}, \mathbf{r}', \omega)$ by calculating the induced charge density distribution iteratively via

$$\rho_{ind}(\mathbf{r}, \omega) = \sum_{i,j} \frac{f(E_i) - f(E_j)}{E_i - E_j - \omega - i\gamma} \psi_i^*(\mathbf{r}) \times \psi_j(\mathbf{r}) \int \psi_i(\mathbf{r}') \phi_{tot}(\mathbf{r}', \omega) \psi_j^*(\mathbf{r}') d\mathbf{r}', \tag{6}$$

with $\phi_{tot}(\mathbf{r}', \omega) = \phi_{ind}(\mathbf{r}', \omega) + \phi_{ext}(\mathbf{r}', \omega)$. The integrals are evaluated using a fourth-order formula obtained from a combination of Simpson's rule and Simpson's 3/8 rule. Equations (5) and (6) are solved self-consistently by iterating $\phi_{ind}(\mathbf{r}, \omega)$ and $\rho_{ind}(\mathbf{r}, \omega)$. This procedure typically converges in three to eight steps when starting with $\phi_{ind}(\mathbf{r}, \omega)=0$, depending on the proximity to a resonance and on the value of the damping constant γ, which throughout this paper is chosen as $\gamma=0.08t$. A much better performance can be achieved when the initial $\phi_{ind}(\mathbf{r}, \omega)$ is taken as the solution of a previously solved nearby frequency. Upon its convergence, the frequency and spatial dependence of the induced electric field and the induced energy are obtained using

$$\mathbf{E}_{ind}(\mathbf{r}, \omega) = -\nabla \phi_{ind}(\mathbf{r}, \omega) \tag{7}$$

and

$$U_{ind}(\omega) = \int |\mathbf{E}_{ind}(\mathbf{r}, \omega)|^2 d\mathbf{r}. \tag{8}$$

The observed resonances in the induced energy and charge density distribution at certain driving frequencies of the applied electric field correspond to collective modes of the cluster.

In the following, the local induced charge density distribution is used for analyzing the characteristic spatial modulation of a given plasmonic resonance. The energy scale is given in terms of the tight-binding hopping parameter t and $\hbar=1$.

III. RESULTS

Let us first focus on the dielectric response function in linear chains of atoms, with the intent to identify the basic features of their collective excitations. Unless otherwise stated, the interatom spacing is fixed to $a=3r_B$, where r_B is the Bohr radius, and the number of atoms in the chain is varied. The frequency dependence of the induced energy in such systems, exposed to a driving electric field along the chain direction, is shown in Fig. 1(a). It exhibits a series of resonances, which increase in number for chains with in-

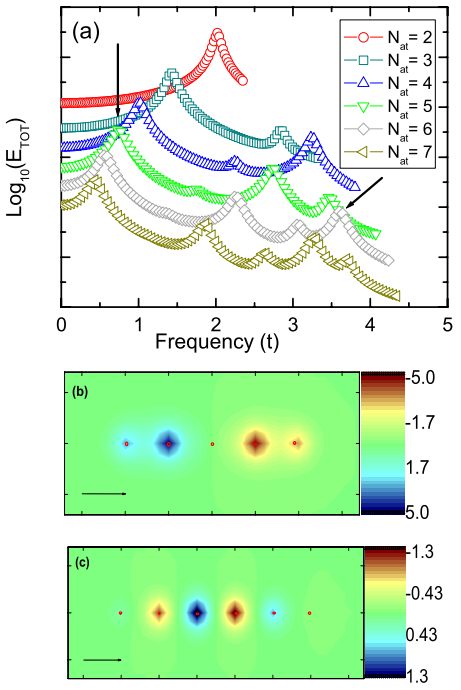

FIG. 1. (Color online) Longitudinal modes in atomic chains. (a) Decimal logarithm of the total induced energy (artificially offset) as a function of the frequency of an external electric field which is applied along the direction of the chain. The resonance peaks correspond to different modes. The arrows indicate the peaks for which the corresponding charge density profiles are shown in (b) and (c). (b) Induced charge density distribution for the lowest-energy mode at $\omega=0.73t$ in the five-atom chain. (c) Induced charge density distribution for the highest-energy mode at $\omega=3.56t$ in the six-atom chain. In (b) and (c) the arrows indicate the direction of the external applied electric field.

creasing length. As observed in the spatial charge density distribution, e.g., shown for the five-atom chain in Fig. 1(b), the lowest peak corresponds to a dipole resonance. When increasing the system size N, there are more electronic levels available in the spectrum of the system and the spacing between them decreases, i.e.,

$$E_{n+1} - E_n = 4t \sin\left(\frac{\pi}{2N+2}\right)\sin\left(\frac{2n\pi+\pi}{2N+2}\right) \underset{N\gg 1}{\propto} \frac{1}{N^2}. \quad (9)$$

Since the dipole resonance frequency is associated with the transition between the highest occupied and the lowest vacant energy level, it also decreases for larger chains, as observed in Fig. 1(a). The resonances at higher frequencies correspond to higher harmonic charge density distributions. For example, in Fig. 1(c), we show the charge density distribution corresponding to the highest frequency resonance of the six-atom chain. In contrast to the dipole resonance, these modes show a rapidly oscillating charge density distribution and thus have the potential to provide spatial localization of collective excitations in more sophisticated structures. While an extension to much larger chains is numerically prohibitive within the current method, the finite-size scaling of the observed dielectric response of these clusters indicates that the

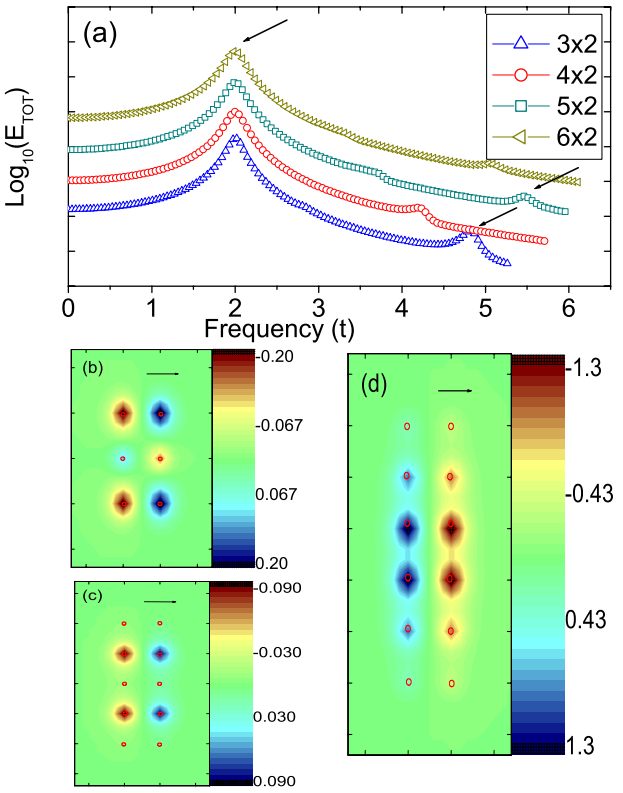

FIG. 2. (Color online) Transverse modes in coupled chain structures. (a) Logarithm of the total induced energy (artificially offset) as a function of the frequency of an external electric field applied transversely to the chain. The low-energy mode is central, the analog of a bulk plasmon, and the high-energy mode is located at the surface, the analog of a surface plasmon. The arrows indicate the peaks for which the corresponding charge density profiles are shown in the other insets. (b) Induced charge density distribution for the mode at $\omega=4.91t$ in the three-atom double chain. (c) Induced charge density distribution for $\omega=5.41t$ in the five-atom double chain. (d) Induced charge density distribution for $\omega=1.93t$ in the six-atom double chain. In (b)–(d) the arrow indicates the direction of the external applied electric field.

frequency of the dominant low-energy plasmon mode scales as $\Delta E \propto 1/N^2$, consistent with the discussion above.

In order to study the transverse collective modes we apply an external electric field perpendicular to ladder structures made of coupled linear chains of atoms.[13] Figure 2(a) shows that for every chain size there are two resonance peaks for the total induced energy, the higher energy is an end mode, as shown in Figs. 2(b) and 2(c) for the three- and five-atom double chains, respectively, whereas the lower-energy peak corresponds to a central mode, as displayed in Fig. 2(d) for the six-atom double chain. It is also confirmed that as the length of the chain is increased, the central mode gets stronger relative to the end mode, which is the expected behavior for bulk versus surface excitations. These results are in agreement with the findings in Ref. 14.

Let us next examine what happens when the direction of the external electric field is varied. Figure 3 shows the dielectric response of a 4×6-atom rectangular structure for different angle incidence directions of the applied field. When the field is parallel to one of the edges ($\theta=0°$ or

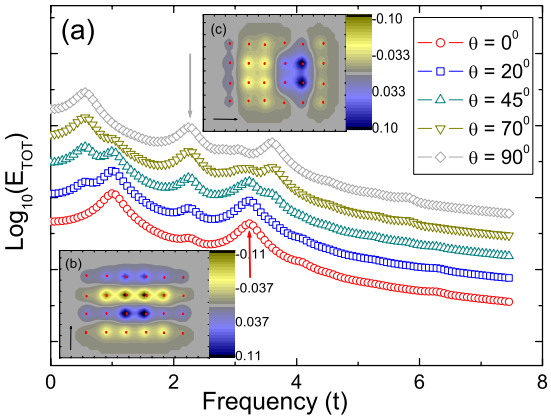

FIG. 3. (Color online) Dependence on the direction of the applied electric field. (a) Logarithm of the total induced energy (artificially offset) as a function of frequency of external electric fields applied to a 4×6 rectangle at different incident angles. $\theta=0°$ when the field is parallel to the four-atom edge and $\theta=90°$ when it is parallel to the six-atom edge. The arrows indicate the peaks for which the corresponding charge density profiles are shown in the other insets. (b) Induced charge distribution for $\theta=0°$ and $\omega=3.15t$. (c) Induced charge density distribution for $\theta=90°$ and $\omega=2.15t$. In (b) and (c) the arrow indicates the direction of the external applied electric field.

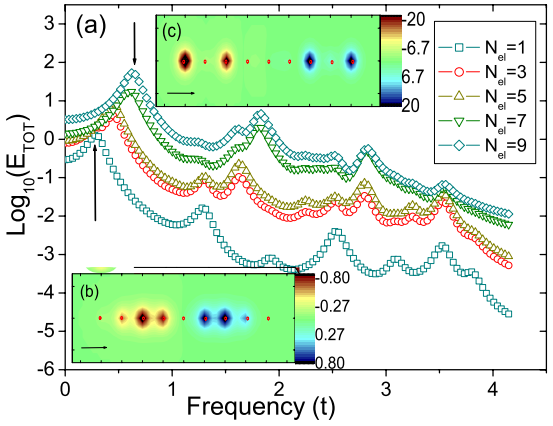

FIG. 4. (Color online) Variation in the number of electrons. (a) Logarithm of the total induced energy as a function of the external electric field frequency. The number of electrons N_{el} in a nine-atom chain is varied. The arrows indicate the modes whose charge density profiles are shown in the other insets. (b) Induced charge density distribution for $N_{el}=1$ at $\omega=0.36t$. (c) Induced charge density distribution for $N_{el}=9$ at $\omega=0.53t$. In (b) and (c) the arrow indicates the direction of the external applied electric field.

$\theta=90°$), the response is essentially that of a single chain with the same length, shown in Fig. 1(a). Also the induced spatial charge density modulations are analogous to those of the correspondent linear chain, which can be seen in Figs. 3(b) and 3(c). At intermediate angles the response is a superposition of the two above cases, changing gradually from one extremum to the other as the angle is changed. Notice, for instance, that as the angle increases, the peak at the same frequency of the four-atom dipole resonance diminishes, while simultaneously another resonance is formed at the frequency of the dipole mode of a six-atom chain when the angle is tuned from $\theta=0°$ to $\theta=90°$. For $\theta=0°$ there is only the peak at the frequency of the four-atom chain dipole resonance, whereas for $\theta=90°$ only the dipole peak corresponding to the six-atom dipole frequency is present. The superposition of the responses from each direction is a consequence of the linear response approximation employed since the response is a linear combination of those obtained from each direction component of the external field.

Next, let us analyze the dependence of the resonance modes on the number of electrons in the cluster. Figure 4(a) shows significant changes in the response of a nine-atom chain with the external field applied along its direction. In particular, it is observed that the response is stronger when there are more electrons in the sample, a quite obvious fact since there are more particles contributing to the collective response. Moreover the resonance frequencies of lower modes increase with the number of electrons, which can be understood as a consequence of the one-dimensional tight-binding density of states being smallest at the center of the band. Hence the energy levels around the Fermi energy are more sparse in the finite system, and therefore the excitations require larger frequencies at half-filling. The same does not hold for higher frequency modes since these correspond to transitions between the lowest and highest levels for any number of electrons in the sample. Therefore these modes have the same frequency, independent of the electronic filling. Higher filling also allows the induced charge density to concentrate closer to the boundaries of the structure, as a comparison between Figs. 4(b) and 4(c) demonstrates. Figure 4(b) shows that a nine-atom chain with $N_{el}=1$ electron has its induced charge density localized around the center of the chain. In contrast, Fig. 4(c) displays the induced charge density localized at the boundaries of the same structure with $N_{el}=9$. This concentration closer to the surface happens because higher-energy states have a stronger charge density modulation than the lower-energy ones. Therefore the induced charge density is more localized for higher fillings because at low fillings the excitations responsible for the induced charge density are between the more homogeneous lower-energy levels. This can be interpreted as a finite-size rendition of the fact that by increasing the electronic filling one obtains the classical response with all the induced charge density on the surface of the object.

Access to high-energy states is very important for achieving spatial localization of the induced charge density, as the next example shows. In order to find a structure with spatially localized plasmons we consider two parallel eight-atom chains connected to each other by an extra atom at the center. When an external electric field is applied transversely to the chains, the electrons are stimulated to hop between them, but this is only realizable through the connection, therefore the plasmonic excitation is sharply localized around it. Figure 5(a) shows the response of two eight-atom chains; Figs. 5(b) and 5(c) show the induced charge density for the dipole and the highest modes, respectively. It is seen that the induced charge density of the lowest frequency mode is spread along the chains, whereas the high frequency plasmon is more localized since it corresponds to excitations to the highest-energy state that has a large charge modulation as it was pointed out before.

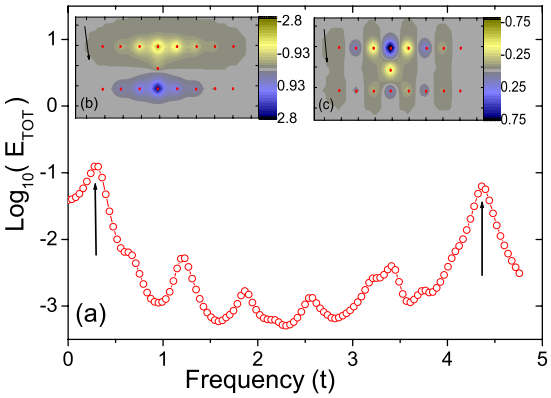

FIG. 5. (Color online) Connection between two chains, $N_{el}=1$. (a) Logarithm of the total induced energy as a function of the frequency of an external electric field applied to two eight-atom chains with an extra atom connecting them at the center. The arrows indicate the peaks for which the corresponding charge density profiles are shown in the other insets. (b) Induced charge density distribution for $\omega=0.28t$. (c) Induced charge density distribution for $\omega=4.36t$. In (b) and (c) the arrow indicates the direction of the external applied electric field.

Let us finally analyze the dependence of the various dielectric response modes on the interatomic distance. Now we consider a fixed number of atoms in the chain but the interatom distance is changed. The dipole moment of the chain is proportional to its length and consequently also proportional to the distance between atoms. Hence one would naively expect that the strength of the dielectric response is strictly proportional to the atomic spacing. However, higher frequency modes require that the electrons are able to hop quickly along the chain in order to produce the fast charge oscillations of the mode. Hence the oscillator strength of the high frequency modes is suppressed for systems where electrons cannot move fast enough. In the tight-binding model, the hopping rate is determined by the hopping parameter t and stems from the overlap of the atomic orbitals on different sites, which decreases with increasing spacing between atoms.[15] Therefore the high frequency modes are suppressed for chains with large interatom spacing because the hopping is so weak that it overcomes the gain coming from a larger dipole moment. On the other hand the oscillator strength of the slow modes increases for larger spacings because they do not require fast motion of electrons along the chain. In this case, the contribution from a larger dipole moment dominates over the suppression due to the smaller hopping rates. This fact is demonstrated in Fig. 6 where the response of seven-atom chains with different atomic spacings is shown. The tight-binding hopping parameter t changes with the atomic spacing a, and here we considered a generic[15] power-law dependence $t \sim a^{-3}$. Comparing the oscillator strength of the slowest mode for all the different spacings, we see that $a=4r_B$ has the strongest response, while $a=2.5r_B$ has the weakest. On the other hand, for the fastest mode we see that the chain with spacing $a=2.5r_B$ has the strongest response, while the chain with $a=4r_B$ has such a small response that we cannot see a peak because it is washed out by other peaks.

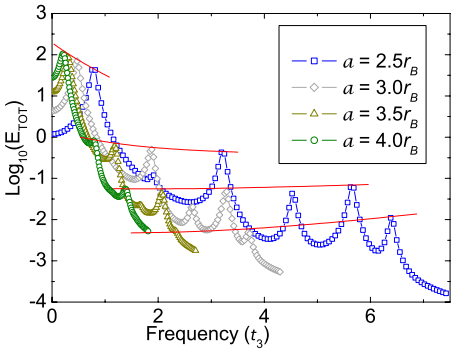

FIG. 6. (Color online) Variation in the distance between neighbor atoms a. Logarithm of the total induced energy as a function of the frequency of an external electric field applied to seven-atom chains with different spacings between atoms a in units of the Bohr radius r_B. The damping constant γ is kept constant for all the different atomic spacings. In this figure the frequency unit is t_3, the tight-binding hopping parameter for $a=3r_B$. The thin red lines connect corresponding peaks for systems with different interatom spacings, indicating that the oscillator strength of the dominant low-energy mode decreases with decreasing spacing, whereas the peaks of the higher-energy modes increase.

IV. CONCLUSION

In conclusion, we have analyzed the evolution of plasmonic resonances in small clusters as a function of the system shape, applied external fields, electron filling, and atomic separation. Using a fully quantum-mechanical nonlocal response theory, we observe that longitudinal and transverse modes are very sensitive to these system parameters. This is reflected in their frequency, oscillator strength, and the spatial modulation of the induced charge density. Specifically, we identify bulk and surface plasmonic excitations which can be controlled in amplitude and frequency by the cluster size. Furthermore, we observe a nontrivial filling dependence, which critically depends on the electronic level spacing in a given structure. We also find that changes in atomic spacings have a very different impact on low-energy vs high-energy modes. And we see that changing the position of a single atom in a nanostructure can completely alter its collective dielectric response. This strong sensitivity to small changes is the key to controlling the modes of ultrasmall structures, and it can thus become the gateway to a new generation of quantum devices which effectively utilize quantum physics for new functionalities.

ACKNOWLEDGMENTS

We would like to thank Gene Bickers, Richard Thompson, Vitaly Kresin, Aiichiro Nakano, and Yung-Ching Liang for useful conversations. We also acknowledge financial support by the Department of Energy (Grant No. DE-FG02-06ER46319). The numerical computations were carried out on the University of Southern California high-performance computer cluster.

*rmuniz@usc.edu

[1] V. V. Kresin, Phys. Rep. **220**, 1 (1992); K. D. Bonin and V. V. Kresin, *Electric-Dipole Polarizabilities of Atoms, Molecules and Clusters* (World Scientific, Singapore, 1997).

[2] G. V. Nazin, X. H. Oiu, and W. Ho, Science **302**, 77 (2003); G. V. Nazin, X. H. Qiu, and W. Ho, Phys. Rev. Lett. **90**, 216110 (2003); N. Nilius, T. M. Wallis, M. Persson, and W. Ho, *ibid.* **90**, 196103 (2003); N. Nilius, T. M. Wallis, and W. Ho, Science **297**, 1853 (2002).

[3] J. Homola, S. S. Yee, and G. Gauglitz, Sens. Actuators B **54**, 3 (1999).

[4] C. R. Moon, L. S. Mattos, B. K. Foster, G. Zeltzer, W. Ko, and H. C. Monoharan, Science **319**, 782 (2008).

[5] D. J. Bergman and M. I. Stockman, Phys. Rev. Lett. **90**, 027402 (2003).

[6] A. K. Sarychev and V. M. Shalaev, *Electrodynamics of Metamaterials* (World Scientific, Singapore, 2007).

[7] I. Grigorenko, S. Haas, and A. F. J. Levi, Phys. Rev. Lett. **97**, 036806 (2006); A. Cassidy, I. Grigorenko, and S. Haas, Phys. Rev. B **77**, 245404 (2008); I. Grigorenko, S. Haas, A. V. Balatsky, and A. F. J. Levi, New J. Phys. **10**, 043017 (2008).

[8] J. C. Slater and G. F. Koster, Phys. Rev. **94**, 1498 (1954); C. M. Goringe, D. R. Bowler, and E. Hernndez, Rep. Prog. Phys. **60**, 1447 (1997); N. W. Ashcroft and N. D. Mermin, *Solid State Physics* (Thomson Learning, New York, 1976).

[9] G. Mie, Ann. Phys. **330**, 377 (1908).

[10] D. M. Wood and N. W. Ashcroft, Phys. Rev. B **25**, 6255 (1982); M. J. Rice, W. R. Schneider, and S. Strassler, *ibid.* **8**, 474 (1973); Q. P. Li and S. Das Sarma, *ibid.* **43**, 11768 (1991); D. R. Fredkin and I. D. Mayergoyz, Phys. Rev. Lett. **91**, 253902 (2003).

[11] S. Nie and S. R. Emory, Science **275**, 1102 (1997).

[12] W. H. Press, B. P. Flanney, S. A. Teukolsky, and W. T. Vetterling, *Numerical Recipes* (Cambridge University Press, Cambridge, 1988).

[13] Within the current approach, at least two coupled chains are necessary to visualize charge redistributions along the transverse direction since charge fluctuations within the orbitals are not accounted for.

[14] J. Yan, Z. Yuan, and S. Gao, Phys. Rev. Lett. **98**, 216602 (2007).

[15] W. A. Harrison, *Electronic Structure and the Properties of Solids* (Freeman, San Francisco, 1980).